Applied Thermal Engineering 258 (2025) 124631

Contents lists available at ScienceDirect

Applied Thermal Engineering

journal homepage: www.elsevier.com/locate/apthermeng

Research Paper

# Experimental and machine learning study on the influence of nanoparticle size and pulsating flow on heat transfer performance in nanofluid-jet impingement cooling

Emmanuel O. Atofarati [a,*], Mohsen Sharifpur [b,c,d,*], Zhongjie Huan [a], Olushina Olawale Awe [e], Josua P. Meyer [f]

[a] Department of Mechanical and Mechatronics Engineering, Tshwane University of Technology, Pretoria, Private Bag X 680, Pretoria 0001, South Africa
[b] Department of Mechanical and Aeronautical Engineering, University of Pretoria, Pretoria, Private Bag X20, Hatfield 0028, South Africa
[c] School of Mechanical, Industrial and Aeronautical Engineering, University of the Witwatersrand, Private Bag 3, Wits 2050, South Africa
[d] Medical Research Department, China Medical University Hospital, China Medical University, Taichung, Taiwan
[e] Statistical Learning Lab, Federal University of Bahia, El Salvador
[f] Department of Mechanical and Mechatronic Engineering, Stellenbosch University, Stellenbosch, South Africa

ARTICLE INFO

*Keywords:*
PV cell
Pulsating jet impingement
Heat transfer
Hybrid nanofluids
Particle size

ABSTRACT

Maximizing heat transfer efficiency is crucial for enhancing performance and durability in diverse engineering applications, including fuel cells, EV batteries, and solar PV/T systems, thereby advancing sustainable energy innovation. This study investigates thermal dissipation from a simulated heat sink aligned with a PV cell's back plate via jet impingement cooling. Specifically, it examines the impacts of pulsatile cooling and nanoparticle size in hybrid nanofluids, comprising combinations of $Al_2O_3$ and MWCNT in water, with varied nanofluid volume fraction (0.05 vol% $\leq \phi \leq$ 0.3 vol%) and flow Reynolds number (15000 $<$ Re $<$ 40000). Key findings reveal significant influences of nanoparticle size, nanofluid concentration, and pulsating flow on heat transfer performance. Notably, sample D demonstrated the highest heat transfer enhancement, achieving approximately 52.94 % and 79.06 % improvement in continuous and pulsating jet cooling compared to de-ionized water under continuous jet cooling. Machine learning classifiers were employed to identify critical thermal performance parameters, with Reynolds number identified as the most significant factor influencing heat transfer. Random Forest and Gradient Boosting classifiers showed notable accuracy in predicting Nu, emphasizing the role of machine learning techniques in optimizing thermal management strategies for improved heat dissipation from solar PV cell backplates.

## 1. Introduction

In pursuing the ambitious 2050 Net Zero Emission goal, the global focus has gravitated towards harnessing solar power for both electrical and thermal energy generation. Solar Photovoltaic (PV) cells are pivotal in this transformative journey. Despite their significance, research indicates that more than 70 % of the energy captured by solar cells is lost as heat [1]. This underscores the urgency for an efficient method to dissipate and utilize this thermal energy for various domestic and commercial applications. Nanofluid jet impingement is renowned for its prowess in eradicating hotspot surfaces through the impressive combination of exceptional heat and mass transfer rates of jet cooling coupled with improved nanofluid thermal conductivity. Several studies have delved into experimental and numerical exploration aimed at harnessing the full potential of solar energy, optimizing heat dissipation, and propelling us closer to a sustainable and emission-free future. Some of these studies are targeted towards utilization of heat-exchanging serpentine pipe [2], pin–fin [3], micro-/mini- channels [4], PV-leaf [5], jet impingement [6] incorporated with heat sinks placed on the back plate of the PV cells.

Some articles have investigated heat transfer performance in water and air jet impingement systems. Akdag et al. [7], examined synthetic annular jet impingement on a flat surface, focusing on variables such as jet-to-surface distance, Reynolds number, and oscillation amplitude (i.e. Womersley number (*Wo*)) using air jets. Their research revealed that synthetic jets, as turbulence promoters, significantly enhance heat transfer compared to circular and annular jets, with the greatest

* Corresponding authors.
*E-mail addresses:* atofarati4excellence@gmail.com, atofaratieo@tut.ac.za (E.O. Atofarati), mohsen.sharifpur@wits.ac.za (M. Sharifpur).

https://doi.org/10.1016/j.applthermaleng.2024.124631
Received 29 May 2024; Received in revised form 31 August 2024; Accepted 10 October 2024
Available online 12 October 2024

**Nomenclature**

*Symbols*

| | |
|---|---|
| T | Temperature ℃ or K |
| D or d | Diameter mm |
| h | Heat transfer coefficient W/mˆ2•K |
| $c_p$ | Specific heat J/kg•K |
| $\dot{q}$ | Heat flux W/mˆ2 |
| k | Thermal conductivity W/m•K |
| U | Velocity m/s |

*Dimensionless Parameters*

| | |
|---|---|
| Re | Reynolds number |
| Pr | Prandtl number |
| Nu | Nusselt number |
| H/D | Dimensionless Nozzle-to target gap / nozzle diameter |
| θ | Dimensionless transient surface temperature |

*Greek Letters*

| | |
|---|---|
| μ | Dynamic viscosity kg/m•s |
| ρ | Density kg/mˆ3 |
| ϕ | Volume fraction % |

*Subscripts*

| | |
|---|---|
| b | Bulk fluid |
| bf | Base fluid |
| nf | Nanofluid |
| c | Copper |
| e | Exit |
| i | index |
| np | Nanoparticle |
| Th | Thermocouple |
| wt | Weighted |

*Abbreviations*

| | |
|---|---|
| DI | De-ionized |
| HTC | Heat transfer coefficient |
| HTF | Heat transfer fluid |

improvement observed under specific conditions. For instance, at a jet-to-surface distance of $H/D = 2$, oscillation amplitude $Wo = 94$, and Reynolds number $Re = 50000$, synthetic jets achieved up to 27 % better heat transfer than circular jets. In a related study, Akdag et al. [8], utilized artificial neural networks (ANNs) to predict heat transfer on a flat plate subjected to a transversely pulsating jet. The ANN model demonstrated high accuracy, with predictions showing less than 1 % deviation from experimental results, highlighting the effectiveness of ANNs in modeling pulsating jet heat transfer.

Additionally, Hofmann et al. [9], investigated the effects of pulsation on flow structure and heat transfer in submerged impinging air jets. They varied pulsation frequency and amplitude across different Reynolds numbers and nozzle-to-plate distances. Their findings indicated that pulsation broadens the jet and reduces its core length due to increased air entrainment, which alters the mean jet velocity. At lower frequencies, the jet behaves similarly to a steady jet, but at higher frequencies (Strouhal number > 0.2), pulsation significantly impacts heat transfer, especially at larger nozzle-to-plate distances. This results in higher heat transfer coefficients at smaller distances but a decrease at larger distances due to enhanced entrainment.

Yadav et al. [10], investigated the mixing and entrainment properties of pulsating jets using particle image velocimetry (PIV) across various parameters. Their study reveals that pulsation affects vortex formation and jet structure, with vortex formation frequency increasing and moving towards the nozzle as pulsation intensifies. The optimal Strouhal number for effective mixing was found to be 0.44 for Reynolds numbers between 3300 and 7500, and pulsation enhances mixing by widening the jet and shortening the potential core, providing insights into the dynamics of turbulent and non-turbulent flow regions. Yadav and Agrawal [11,12], also examined the influence of vortical structure and pulsation frequencies on the near-field behavior of submerged water jets through dye visualization techniques. Their findings indicate that pulsation accelerates mixing and entrainment by destabilizing the shear layer and generating larger vortices, compared to steady jets. The study identifies an optimal pulsation frequency of St = 0.44 for maximizing jet spreading and vortex development, providing insights into the mechanisms that enhance mixing in pulsating jet systems. Despite these insights, studies on pulsating nanofluid jet impingement heat transfer remains limited.

Atofarati et al. [13], offer a detailed review of nanofluid-jet impingement cooling, emphasizing its effectiveness and adaptability in engineering systems. The review explores key factors influencing thermal performance, including jet types (e.g., submerged, free-surface, confined, unconfined, tangential, inclined), as well as effects like crossflow, splattering, nature of the nanofluid and phase change. It also evaluates the role of nozzle design, monojet versus multijet setups, target surfaces, and turbulence promoters (e.g., pulsating jet, synthetic jets). Furthermore, the review highlights various applications of nanofluids and compares existing Nusselt correlations, making it a valuable reference for optimizing this cooling technique.

Javidan et al. [14], conducted an experimental study investigating the impact of single-orifice and multi-orifice nozzle arrays of cooling jets on the hydrothermal and electrothermal performance of PV-modules, utilizing SiC/water nanofluid. The findings reveal that the nanofluid outperformed water in terms of performance. Additionally, the multi-orifice array of nozzles achieved a uniform temperature distribution on the cooled surface, whereas single-orifice nozzles exhibited a better average temperature advantage. Moreover, the researchers noted that the concentration of nanofluid had little significance. In conclusion, they found that nanofluid jet impingement enhances both the hydrothermal and electrothermal performance of PV-modules. Hasan et al. [15], conducted a similar study using SiC/water, $TiO_2$/water, and $SiO_2$/water nanofluids as heat transfer mediums in a single-orifice array of jet-cooled PV-modules. The results indicated that the SiC/water nanofluid exhibited the highest electrical efficiency at 12.75 %, thermal efficiency at 85 %, and an overall combined efficiency of 97.75 %.

Building upon prior research, Suja et al. [16], conducted a numerical investigation into the heat transfer performance of PV-modules cooled by swirling jet impingement, comparing CuO-Water and Al2O3-Water nanofluids using RANS with the SST K-ω turbulent model. Their findings demonstrated superior performance of nanofluids, with $Al_2O_3$-Water nanofluid exhibiting a 116 % performance advantage over CuO at a flow rate of 50 g/min, based on performance evaluation criteria. Selimefendigil and Öztop [17], conducted a numerical study on pulsating rectangular jet impingement with $Al_2O_3$-water nanofluids to evaluate the impact of pulsation frequency, Reynolds number, and nanoparticle volume fraction on heat transfer and fluid flow. Their results indicated that nanoparticles improved heat transfer in steady conditions, increasing the peak Nusselt number and spatially averaged Nusselt number by up to 18.8 % with a 6 % particle volume fraction at Reynolds number 200. However, in pulsating flows, the combined effect of pulsation and nanoparticles did not enhance the stagnation point Nusselt number as effectively as steady conditions, showing less improvement at certain Reynolds numbers and volume fractions.

In a related study, Li et al. [18] conducted a numerical study on the heat transfer and flow structure of $Al_2O_3$-water nanofluids in periodic pulsating slot-jet impingement, comparing rectangular and triangular waveforms. Their findings indicate that triangular waveforms at medium pulsation frequencies, combined with high nanoparticle volume fractions and Reynolds numbers, significantly enhance heat transfer efficiency, though with a trade-off in temperature uniformity. Maatoug et al. [19], proposed the use of pulsating multiple nanofluid jet impingement for cooling solar PV cells. Through numerical simulations, they investigated the comparative impact of pulsating multiple jets of $Al_2O_3$-Water nanofluid (with varying nanoparticle shapes) and Ag/MgO-water nanofluid on the thermal performance of the conductive back plate of PV systems. Utilizing the finite volume method in ANSYS Fluent, their results indicated significant influences of nanoparticle shape, number of slots, pulsating amplitude, and nanoparticle loading on the mean temperature of the conductive plate. They further noted that pulsating amplitude played a more crucial role than pulsating frequency in optimizing heat transfer, resulting in a remarkable 63.5 % enhancement in Nusselt number at the peak pulsating amplitude. Also, Atofarati et al. [20] and Wilken et al. [21], previously conducted experimental verification of optimal hydrodynamic parameters in nanofluid jet impingement cooling. Their findings emphasized the importance of achieving specific ratios, including a height-to-target diameter ratio (H/D) of 4 and a jet diameter-to-surface diameter ratio ($D_{jet}$ / $d_{target}$) of 0.10, alongside high nanofluid volume fraction and coolant flow rate, to achieve optimal thermal dissipation from a hot surface. In a follow-up study, Atofarati et al. [6] investigated and refined the pulsating parameters to boost heat transfer during pulsating nanofluid jet impingement cooling, using γ-$Al_2O_3$-MWCNT/water hybrid nanofluid. The research examined variations in pulsating frequency *(0.2 Hz ≤ F ≤ 20 Hz)*, amplitude *(4 Vp ≤ A ≤ 20 Vp)*, waveform (sine, square, triangular), wave offset *(0 ≤ J ≤ 4)*, and nanofluid concentration *(0.05* vol% *≤ φ ≤ 0.3* vol%*)* to optimize heat transfer. The findings indicated that, except for the waveform, all parameters had a notable impact on heat transfer efficiency, with the highest improvement of 24 % observed using 0.3 vol% $Al_2O_3$-MWCNT/water when compared to continuous jet impingement with deionized water. Furthermore, a 20 % enhancement was achieved with a sine waveform at $\varphi = 0.3$ vol%, $F = 0.2$ Hz, $A = 8$ Vp, and $J = 2$. Contrary to some numerical works suggesting that high pulsating amplitude and frequency result in improved thermal performance, our experimental findings refuted this notion. Instead, we observed that a combination of high nanofluid volume fraction, low pulsating frequency, low pulsating amplitude, and a sine wave form generated the best thermal performance, achieving an impressive enhancement of 24 %.

To the best of our knowledge, no experimental studies have yet investigated the effects of nanoparticle size and pulsating flow on hybrid nanofluid jet cooling, particularly using γ-Al2O3-MWCNT/water as the heat transfer fluid for solar thermal management. Consequently, this experimental investigation is crucial to address this gap in the existing literature.

This study aims to examine the impact of γ-$Al_2O_3$-MWCNT/water hybrid nanofluid on the heat transfer efficiency in jet impingement cooling of simulated heat sink aligned to a solar PV cell conductive back plates with varying particle sizes ($Al_2O_3$: 5 nm & 20 nm, MWCNT: < 7 nm & 30–50 nm), employing pulsating parameters {sine waveform, pulsating frequency $(F = 0.2)$, amplitude $(A = 8)$, and wave offset $(J = 2)$}, as well as Reynold number (15000 < Re < 40000) and nanofluid volume fraction (0.05 vol% ≤ φ ≤ 0.3 vol%). Classification of the key parameters influence the heat transfer during nanofluid jet impingement cooling will be estimated using machine learning classifiers and the prominent parameter will be identified.

**Table 1**
Thermophysical Properties of nanoparticles.

| Thermophysical property | Nanoparticle | Supplier Value |
|---|---|---|
| **Thermal conductivity (W/m.K)** | $Al_2O_3$ | 41 |
| | MWCNT | 2586 |
| **Specific heat (J/kg.K)** | $Al_2O_3$ | 880 |
| | MWCNT | 711 |
| **Mean Density (kg/m3)** | $Al_2O_3$ | 3970 |
| | MWCNT | 2100 |

**Table 2**
Nanofluid Particle Sample Permutation Chart.

| Sample | Particle Size (nm) | | Surfactant |
|---|---|---|---|
| | $Al_2O_3$ | MWCNT | |
| A | 5 | < 7 | Sodium DodecylBenzene Sulfonate (SDBS) |
| B | 20 | < 7 | SDBS |
| C | 20 | 30–50 | SDBS |
| D | 5 | 30–50 | SDBS |
| Supplier | Nanostructured and Amorphous Material Inc., USA | MKnano Company, Canada | Sigma-Aldrich, Germany |

## 2. Experimental Methods

### 2.1. Nanofluids materials and preparation

In this study, hybrid nanofluids of γ-Al2O3 and MWCNT nanoparticle with thermophysical properties described in Table 1 are dispersed in Deionized water were prepared through a two-step technique, resulting in the desired volume fractions (0 vol% ≤ φ ≤ 0.3 vol%). The respective γ-Alumina oxide (Al2O3) nanoparticles and Multi-Walled Carbon Nanotubes (MWCNT) of different nanoparticle sizes were permutated and mixed in a 60:40 ratio as shown in Table 2. The respective samples A, B, C & D were characterized and utilized for the heat transfer study. The blend underwent magnetic stirring for 30 min at a consistent speed, followed by ultrasonication for 1 h utilizing a Qsonica (Q-700) sonicator with a 90 % sonication amplitude, within a constant bath temperature set to 20 °C. Physical observation and viscosity measurement over time at around 30 °C were monitored for about 6 h. The result in Fig. 1**(a)** shows the physical observation of the nanofluid after over 24 h of preparation, while Fig. 1**(b)** shows the viscosity of the respective sample of the γ-Al2O3-MWCNT/water nanofluid. The viscosity value over this time interval shows that the nanofluids had significant stability.

### 2.2. Nanoparticle's morphology

A comprehensive morphological analysis of the γ-Al2O3 and MWCNT nanoparticles, as well as their hybrids was meticulously performed using a Zeiss Crossbeam 540 scanning field emission gun electron microscope (FEG-SEM), available at the Microscopy Department of the University of Pretoria. To ensure precise and detailed observations, the nanoparticle samples underwent thorough preparation before visualization in the FEG-SEM, generating the images presented in Fig. 2. Keen examination of the images of the γ-Al2O3 nanoparticles unveiled a spherical morphology characterized by cloud-like particle agglomerates, while the MWCNT displayed a tubular configuration. These observations are consistent with established literature on nanoparticle morphology, validating their accurate characterization.

### 2.3. Measurement of thermophysical properties

The viscosity and thermal conductivity of hybrid nanofluid samples A, B, C, and D of the γ-Al2O3-MWCNT/water nanofluid were

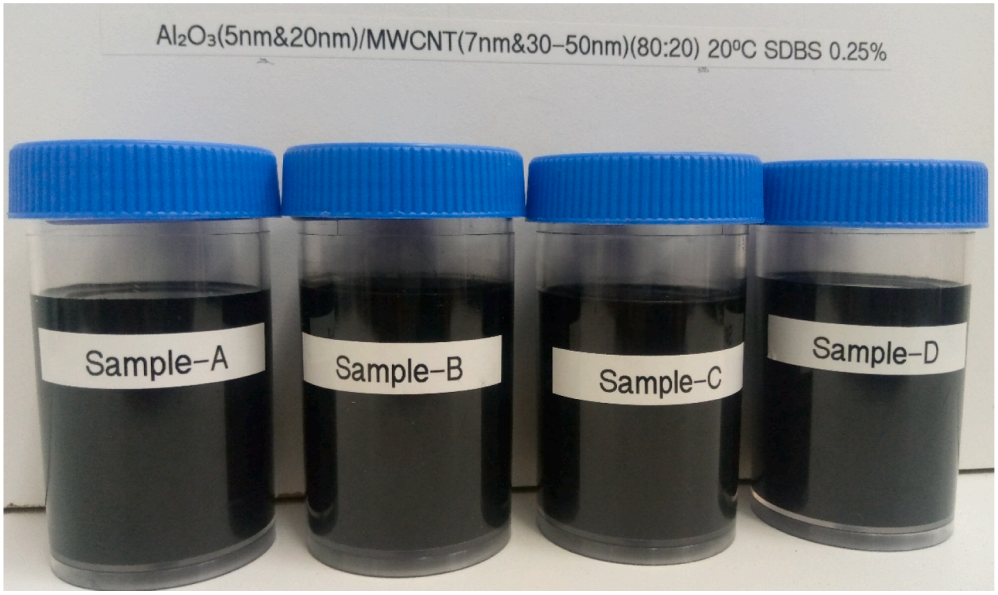


(a)

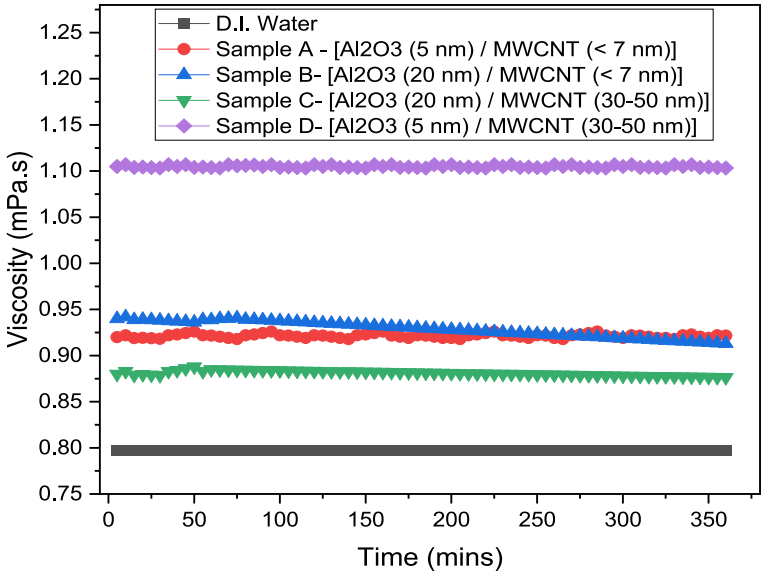


**Fig. 1.** Stability of the nanofluid (a) Physical Inspection (b) Viscosity over time at 30 °C.

determined following the methodology outlined in Atofarati et al. [11]. For viscosity measurement, the SV-10A Vibro-Viscometer was employed, connected to a constant temperature bath spanning from 20 °C to 50 °C. Calibration of the instrument was achieved through a one-point standard calibration procedure using pure water. Then the measured viscosity of the de-ionized water was compared with the values read by Senger & Watson [22]. Subsequently, viscosity readings were obtained for various samples of the nanofluids and compared to those of de-ionized water. As shown in Fig. 3 **(a)**, the results exhibit a consistent decrease in fluid viscosity with increasing temperature for all the samples and de-ionized water. Notably, the γ-Al2O3-MWCNT/water nanofluids samples demonstrated slightly higher viscosity than De-ionized water. Sample D has the highest viscosity which corresponds to an increase in pressure drop in the system and implies the need for higher pump power.

For thermal conductivity measurement, a KD2-Pro thermal analyzing meter by Decagon Devices, USA, with ± 10 % accuracy, was employed over a temperature range of 10 °C to 30 °C. Calibration of the thermal conductivity meter was performed using the standard thermal conductivity fluid (Glycerin). Then the measured thermal conductivity of the de-ionized water was compared with the values read from Yunus & Ghajar [23]. The obtained thermal conductivity readings against temperature change for the various γ-Al2O3-MWCNT/water nanofluid samples and de-ionized water are illustrated in Fig. 3 **(b)**. The results indicate an increase in thermal conductivity with temperature and the γ-Al2O3-MWCNT/water nanofluid had better thermal conductivity than the de-ionized water. Sample C and D had comparatively the best conductivity among others.

For electrical conductivity measurement, a Eutech Con 700 conductivity meter was utilized. Calibration was carried out using the standard conductivity fluid with an average electrical conductivity of 141.36 mS/m at 25 °C. Then electrical conductivity of the nanofluids

and water were measured, and the results are presented in Fig. 3**(c)**. The result shows that the nanofluids generally had much better electrical conductivity than deionized water, with sample D having the highest electrical conductivity.

### 2.4. Experimental setup and procedure

The experimental setup was meticulously designed to simulate the thermal performance of a typical solar PV cell cooling system in an inverted configuration. At the core of the setup is a copper cylindrical block, representing a section of the conductive heat sink typically positioned against the rear surface of a photovoltaic (PV) module, as illustrated in Fig. 4. To generate the necessary thermal load, six 100 W cartridge heaters were securely embedded in the test section. These heaters were insulated using polytetrafluoroethylene (PTFE), ensuring minimal heat loss and precise thermal measurements. In this inverted arrangement, heat is applied from the bottom of the copper block, while the top surface is subjected to cooling, effectively reversing the conventional thermal flow in a PV cooling system. This inversion required adjustments in the calculation of flow and gravitational dynamics, with the gravitational acceleration set to $-9.82\ m/s^2$, consistent with standard PV applications. This configuration enables an accurate evaluation of heat transfer mechanisms under real-world PV cooling scenarios, while offering a controlled environment to examine the effects of flow velocity and gravity on thermal performance.

The experimental apparatus includes a centrifugal pump, ultrasonic flowmeter, pressure transducer, collection tank, single Lechler circular nozzle (3 mm diameter), heat exchanger, control valves, and a pulsating device. The pulsating system comprises solenoid valves (RS PRO Solenoid Valve, 2 ports, NC, 24 V AC/DC), diodes, a function generator (TG120-20 MHz dial-set function generator), and a power supply. Pulsating flow is created by setting the function generator to produce specific waveforms at desired frequencies. This electrical signal is sent to the solenoid valves, which open and close in response to the pulses, generating a pulsating fluid flow. The pulsation frequency and pattern are controlled by adjusting the function generator settings, allowing for precise experimentation and analysis of pulsating flow effects.

The setup also integrates thermocouples, data acquisition systems, and computers. For surface temperature monitoring, three thermocouples are inserted radially at a depth of approximately 3 mm near the top surface. Five T-type thermocouples, mounted on a ring holder with a diameter of around 40 mm, are concentrically placed above the surface to measure the temperature of the exiting cooling fluid. A detailed illustration of the complete setup is provided in Fig. 5.

In this study, the cooling dynamics of a solar PV cell's conductive heat sink are simulated using the flat-top surface of the copper block.

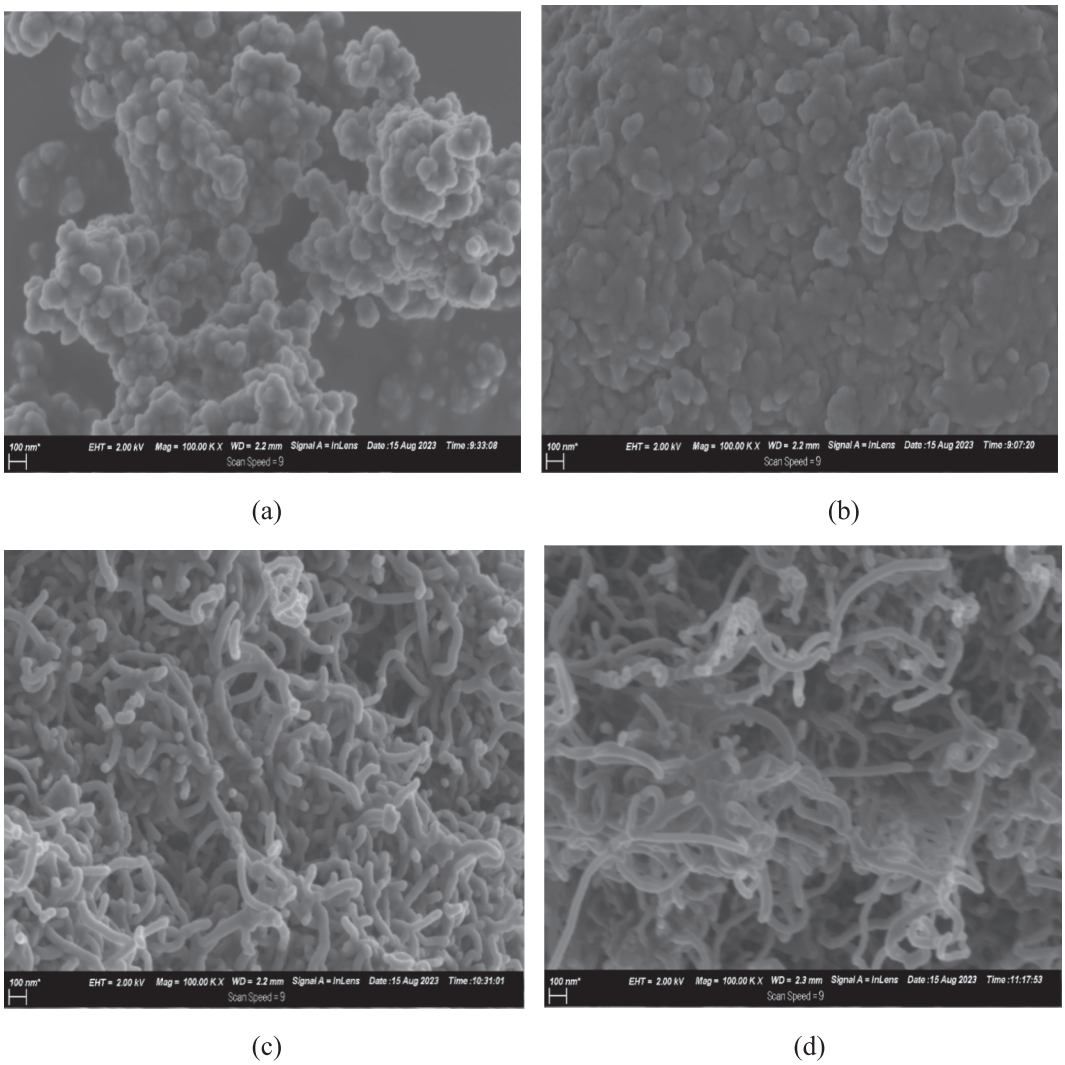


**Fig. 2.** FEG-SEM images of (a) $Al_2O_3$ (5 nm), (b) $Al_2O_3$ (20 nm) (c) MWCNT (< 7 nm) (d) MWCNT (30–50 nm) (e) Sample A- [$Al_2O_3$ (5 nm)/ MWCNT (< 7 nm)], (f) Sample B- [$Al_2O_3$ (20 nm)/ MWCNT (< 7 nm)], (g) Sample C- [$Al_2O_3$ (20 nm)/ MWCNT (30–50 nm)], (h) Sample D- [$Al_2O_3$ (5 nm)/ MWCNT (30–50 nm)], at a Magnification of 100 KX.

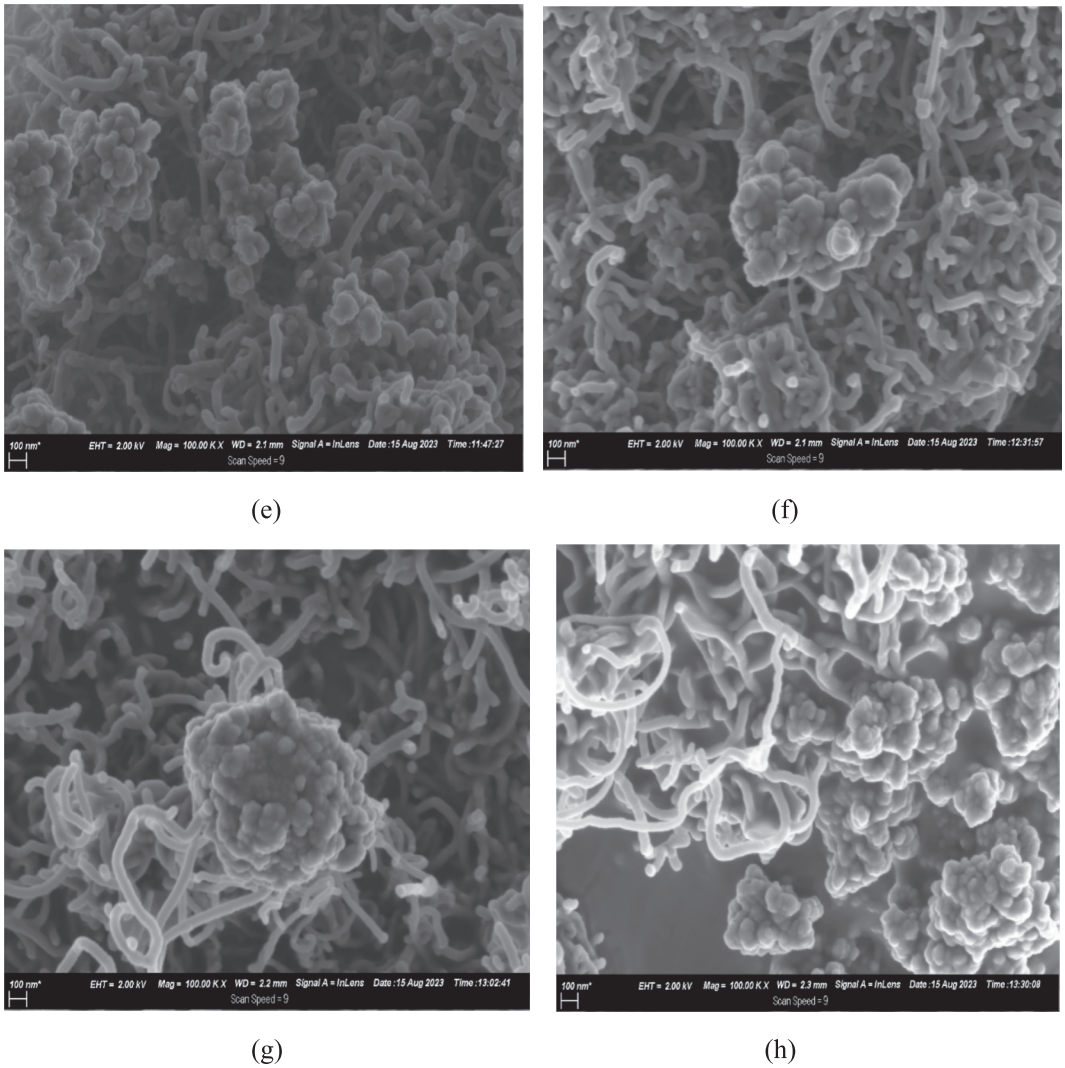


**Fig. 2.** (*continued*).

The transient cooling process of the upper surface, subjected to a fixed heat flux and cooled by either a continuous or pulsating nanofluid jet, is analyzed. The investigation is conducted under quasi-steady-state conditions, comparing the performance of water and γ-$Al_2O_3$-MWCNT/water hybrid nanofluids with varying particle sizes and volume concentrations (a 60:40 mixture of γ-$Al_2O_3$ and MWCNT).

The heat exchanger system uses a tube-in-tube configuration connected to a constant-temperature water bath that circulates water at 28 °C through the test section. This maintains the coolant (water or nanofluid) temperature between 29–31 °C, simulating ambient conditions of 30 °C. Before each experiment, 7.5 L of nanofluid at ambient temperature is introduced into the collection tank. The thermal bath, integrated with a double-pipe heat exchanger, stabilizes the inlet temperature at approximately 30 °C. Once stabilized, the cartridge heaters in the copper block supply constant heat flux, raising the block's temperature to around 80 °C. This setup accurately reflects real-world thermal conditions, allowing for precise analysis of heat transfer performance under controlled cooling parameters.

When pulsating cooling is employed, the pulsating device is activated with optimized pulsating parameters {sine waveform, pulsating frequency (F = 0.2), amplitude (A = 8), and wave offset ($J$ = 2)}, as determined in a previous study [6]. The fluid is pumped from the tank, through the heat exchanger, and onto the target surface at a predetermined flow rate, controlled by a bypass and valve system. During the first 70 s, instantaneous measurements of fluid flow rate, surface temperature, gauge pressure before impingement, and the fluid's exit temperature are recorded using thermocouples, a pressure transducer, a data logger, and a computer interface. The recorded data is then retrieved and subjected to detailed analysis.

### 2.5. Data Reduction and uncertainty

The average impingement Reynolds number (Re), and Peclet number (Pe) were calculated using similar formulae used by Padiyaar et al. [25] and in our previous study, considering the impact of gravity on the jet before impingement on the surface cooled from the base.

$$u_{imp} = \sqrt{(u_{jet})^2 - 2gz} \tag{1}$$

$$D_{imp} = D_{jet}\left(\frac{u_{jet}}{u_{imp}}\right)^{0.5} \tag{2}$$

$$Re = \frac{\rho . u_{imp} . D_{imp}}{\mu} \tag{3}$$

$$Pe = Re_{imp} \times Pr \tag{4}$$

The determination of electrical power ($\dot{Q}_{elect}$) supplied to the heater involves rigorous calculation, accounting for the entirety of heat flow

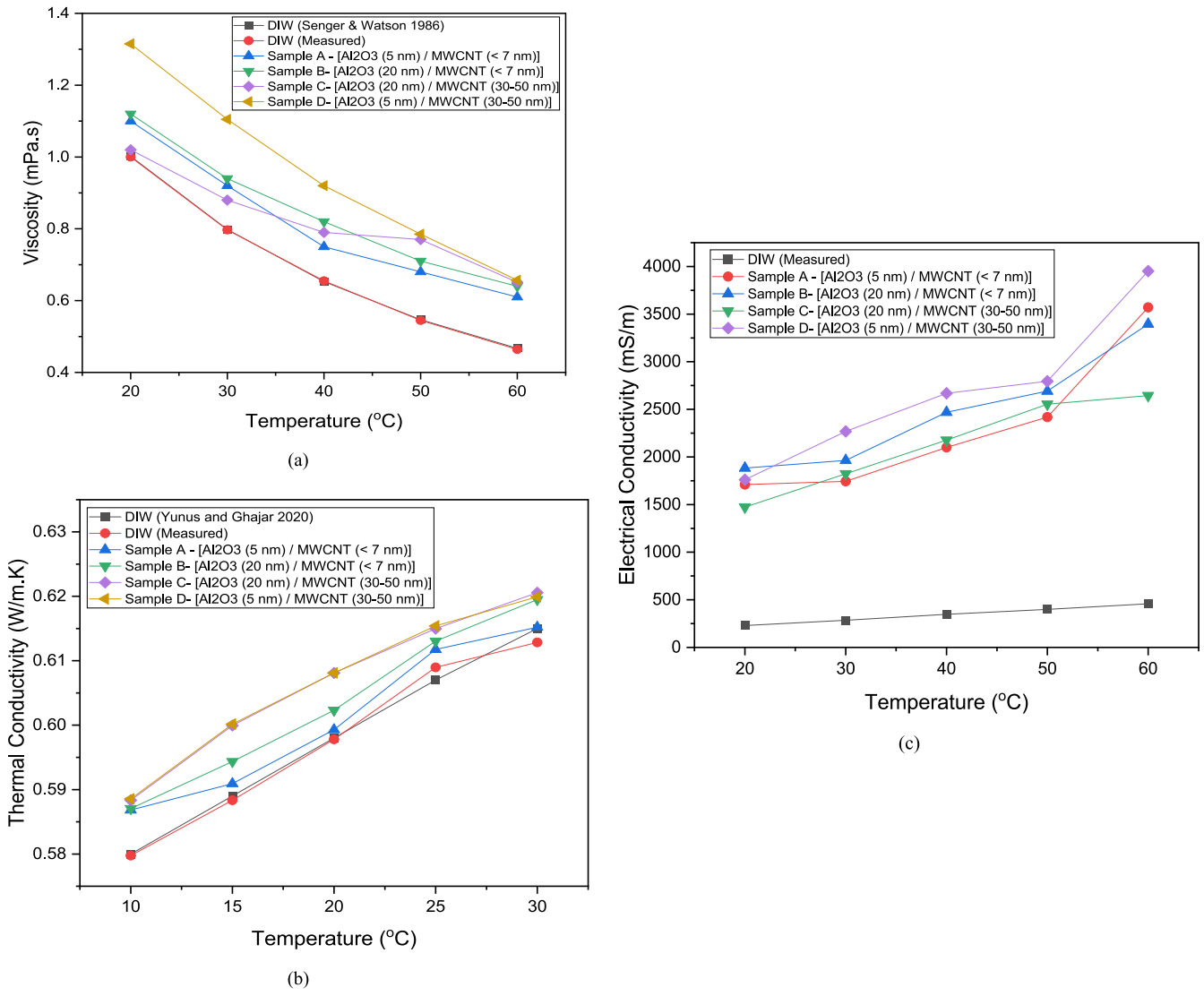


**Fig. 3.** Thermophysical Properties of Nanofluid (a) Viscosity (b) Thermal Conductivity (c) Electrical Conductivity.

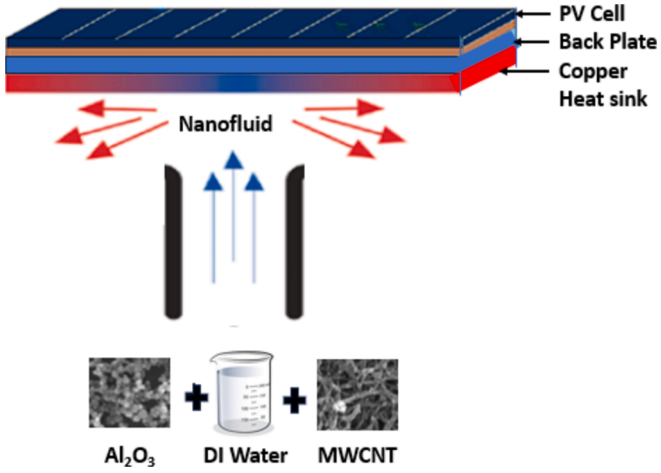


**Fig. 4.** Schematical of Simulated Copper Heat Sink Concept.

introduced into the block. Specifically, it is derived from the heat flux assessment at the target surface, factoring in the diameter of target surface ($D_t$). Employing a precise approximation technique (i.e. the weighted average heat flux method), the measurement of the target surface temperature which is pivotal for accurate analysis was calculated similar to our previous study [20].

$$\dot{q}_{wt} = \frac{\sum_{i=1}^{4}(\Delta y \times \dot{q})_{i,i+1}}{\sum_{i=1}^{4}\Delta y_{i,i+1}} \tag{5}$$

$$T_{t,i} = T_{tc,i} - \frac{\dot{q}_{wt} \times \Delta x_{t,i}}{k_c} \tag{6}$$

$$T_t = \frac{\sum_{i=1}^{5} T_{t,i}}{5} \tag{7}$$

$$T_e = \frac{\sum_{i=1}^{5} T_{e,i}}{5} \tag{8}$$

$$T_{bulk} = \frac{T_{inlet} + T_{exit}}{2} \tag{9}$$

where $T_{in}$ is the temperature of the coolant emitted from the nozzle, $T_e$ is the mean temperature of the coolant leaving the target surface after-

wards, $T_{bulk}$ is the bulk coolant temperature, $T_t$ is the average temperature of the target surface, $\dot{q}_{wt}$ is the weighted average heat flux, $\Delta y_{t,i}$ is the perpendicular distance between the different thermocouples point. The Nusselt number ($Nu_{imp}$) is used to estimate heat dissipated from the surface and the heat transfer performance of the coolant on the target surface.

$$Nu_{fluid} = \frac{\dot{q}_{max} \times D_{jet}}{(T_{bulk}).k} \tag{10}$$

The assessment of uncertainty in both measured and calculated parameters adhered to the methodologies outlined by Moffat [26] and Kline [27]. In quantifying the uncertainty ($\delta x_i$) associated with measuring a single parameter, it is imperative to discern both bias (b) and precision (p) errors. Bias error denotes a constant deviation linked to the instrument's accuracy, typically provided by the manufacturer, whereas precision error encompasses stochastic or human-related discrepancies arising from individual variations, environmental conditions, and measurement location. To determine uncertainty for both individual measurements and overall calculated parameters, Equations (1) and (2) were utilized as prescribed by Kline's methodology. The entire

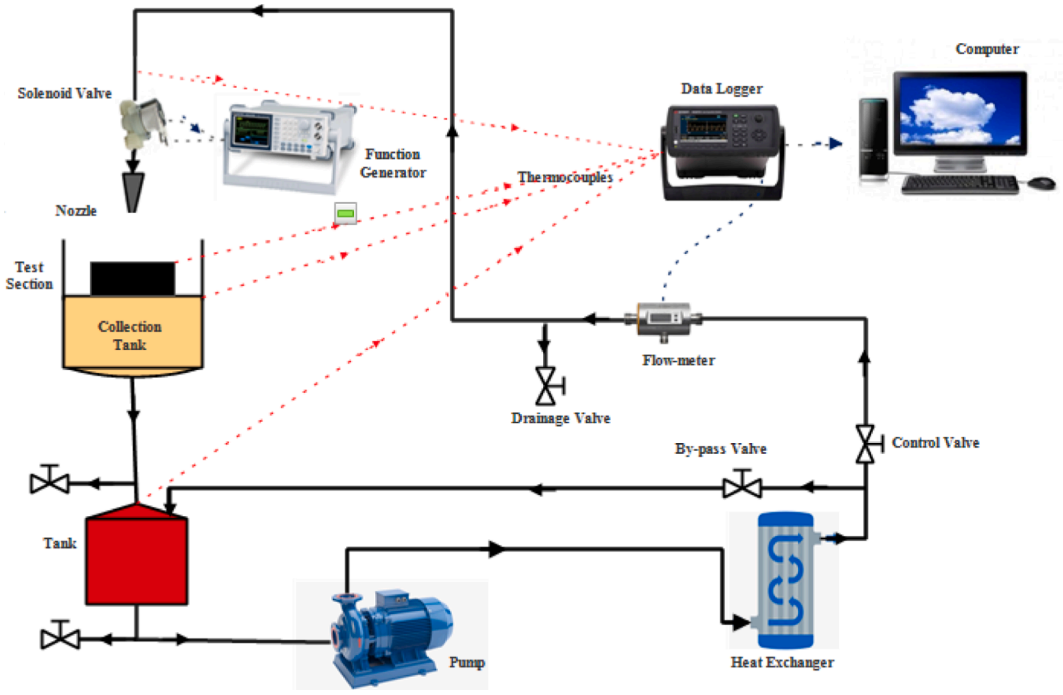


(a)

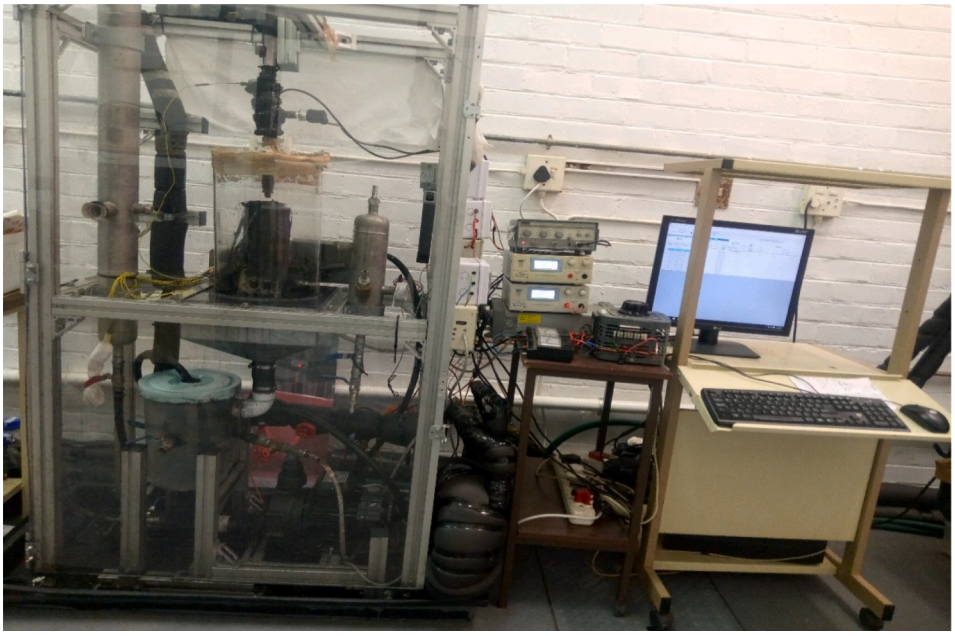

(b)

**Fig. 5.** Experimental Test Rig (a) Schematic diagram (b) Pictorial diagram (c) Test section: tampered copper cylindrical block with position of cartridge heaters (d) Thermocouples positions for surface temperature & exiting fluid temperature [24].

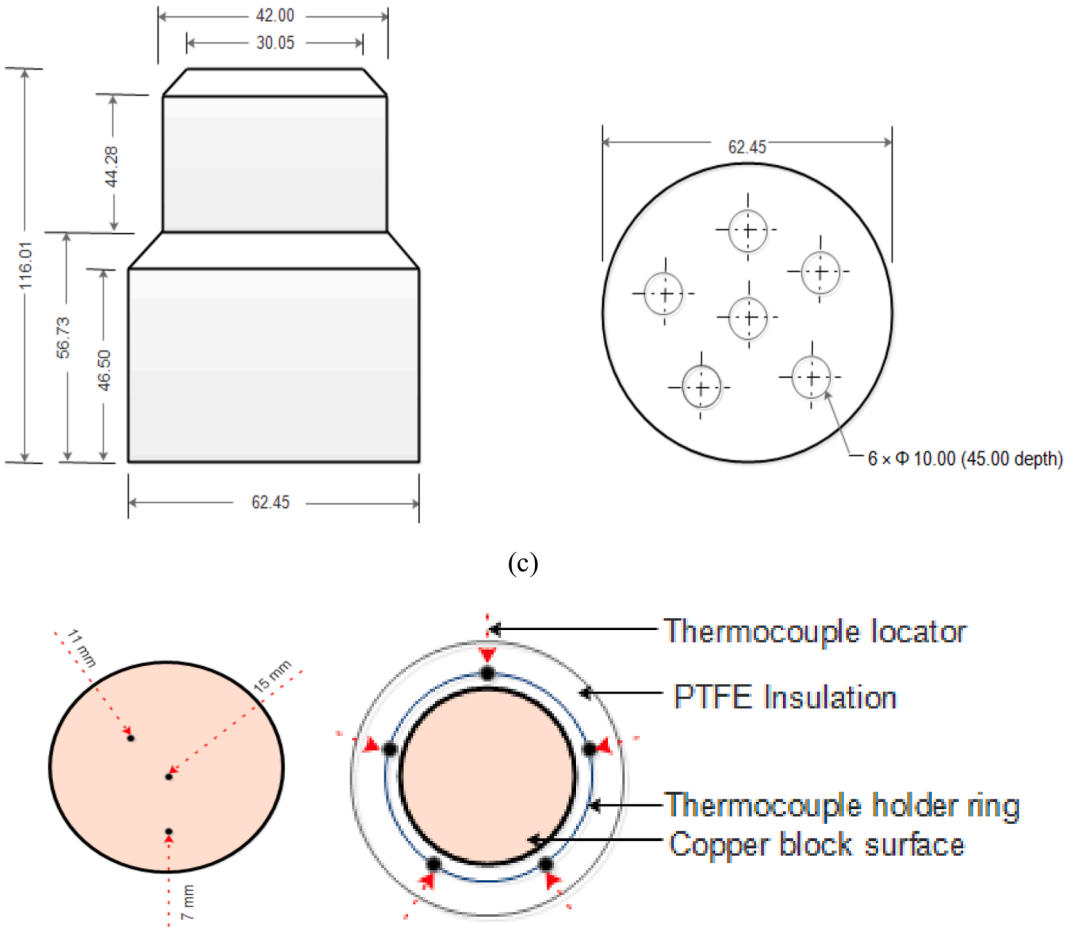


**Fig. 5.** (*continued*).

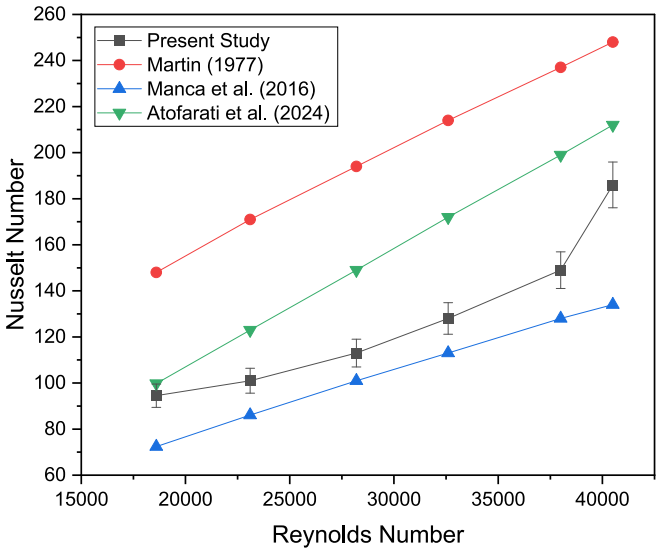


**Fig. 6.** Result validation with other literatures outcome and our previous study.

analysis was conducted using the Python "Uncertainty" function for facilitating the computation of uncertainty within a 95 % confidence interval. The result shows an uncertainty of 0.30 %, 3.56 %, and 5.35 % respectively for temperature readings, Reynolds number, and Nusselt number calculated. Further details on the uncertainty analysis is provided in the work of Atofarati [24].

$$\delta x_i = \left(b_i^2 + p_i^2\right)^{1/2} \tag{11}$$

$$\delta F = \left\{ \left(\frac{\delta F}{\delta x_1}\right)^2 \partial x_1 + \left(\frac{\delta F}{\delta x_2}\right)^2 \partial x_2 + \left(\frac{\delta F}{\delta x_3}\right)^2 \partial x_3 + \cdots + \left(\frac{\delta F}{\delta x_n}\right)^2 \partial x_n \right\}^{1/2} \tag{12}$$

## 3. Results and Discussion

### 3.1. Validation of results

The initial validation of the test rig commenced with an assessment of its findings, comparing them against prior studies involving continuous jet impingement of water across a spectrum of mass flow rates. Subsequent to this comparison, the heat transfer performance results were juxtaposed with those obtained in prior works by Manca et al. [28] Martins. [29] and Atofarati et al. [6]. Fig. 6 presents a graphical representation illustrating the close correspondence between the acquired results and those documented in analogous preceding studies, conducted under similar flow conditions. Notably, the findings reveal a linear correlation between the heat transfer rate (Nusselt number) and the fluid flow Reynolds number, with error bars indicating the range of uncertainty in the Nusselt number values reported in section 2.5. It is worth noting that slight deviations from our previous work (Atofarati et al [6]) were observed, attributable to modifications made to the test rig and variations in ambient conditions during the respective experimentation.

The time series behavior of flow velocity under standard pulsating flow conditions, represented by a sine waveform with pulsation

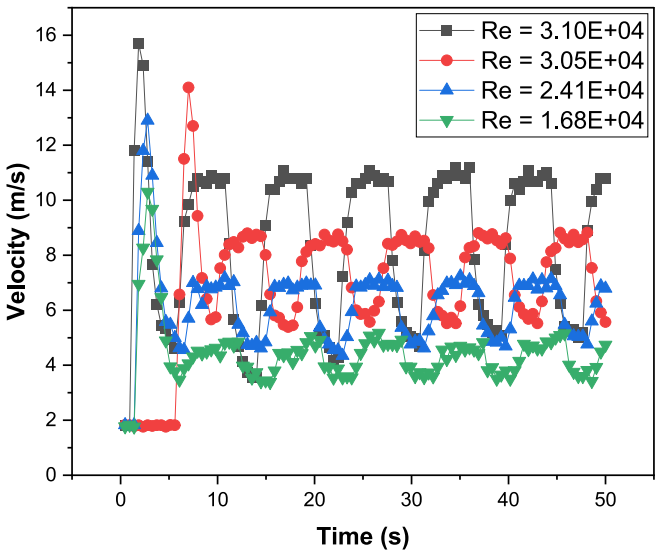


**Fig. 7.** Pulsating flow velocity at various Reynolds numbers.

parameters of frequency (F = 0.2), amplitude (A = 8), and wave offset (*J* = 2), is illustrated in Fig. 7. The graph reveals distinct flow patterns and amplitude fluctuations as the Reynolds number increases. Higher Reynolds numbers exhibit more pronounced and frequent peaks in velocity amplitude, indicating stronger pulsation effects, while lower Reynolds numbers display more stable flow with smaller amplitude variations. These insights are essential for understanding the impact of pulsating flow dynamics on thermal transfer efficiency.

### 3.2. *Nanoparticle size impact on thermal performance*

The study involved examining a 0.3 vol% volume fraction of the γ-$Al_2O_3$-MWCNT/water (60:40) hybrid nanofluid, designated as samples 'A-D', which were prepared with varied combinations of nanoparticle sizes as previously detailed. These assessments were conducted while employing the respective nanofluids as coolants within a continuous jet impingement cooling system. The outcomes, illustrated in Fig. 8 **(a) and (b)**, reveal that sample 'D' demonstrates superior heat transfer performance with increasing flow Reynolds numbers. This trend aligns with the electrical and thermal conductivity characteristics of the fluid, as evidenced in Fig. 3 **(b) and (c)**.

Upon detailed examination of the nanofluid samples, a consistent trend emerges, indicating that samples D and C exhibit progressively superior heat transfer performance with increasing mass flow rate. Intriguingly, both samples are characterized by larger-sized MWCNT particles. This observation is particularly noteworthy, given that the hybridization mixing ratio favors a higher fraction of $Al_2O_3$ over MWCNT. Despite this, the superior thermal conductivity of MWCNT compared to $Al_2O_3$ suggests that the enhanced heat transfer performance (Nusselt number) observed in samples 'D' and 'C' can be attributed to the larger particle size of MWCNT, despite its lower fraction in the hybridization mixing ratio.

Similar trend can be observed in Fig. 8 **(b)**, where the heat transfer coefficient increases proportionally with the Peclet number. The Peclet number, a vital concept in fluid mechanics, delineates the balance between convective and diffusive transport in fluid flow systems, particularly pertinent in nanofluidic processes. Serving as a dimensionless parameter, it quantifies the relative influence of convection, driven by the fluid's motion, versus diffusion, arising from particles' random movement within the fluid. Mathematically expressed as the ratio of convective flux to diffusive flux, it elucidates how fluid flow is governed by these mechanisms, with convective flux reflecting bulk fluid motion and diffusive flux representing particle movement induced by molecular

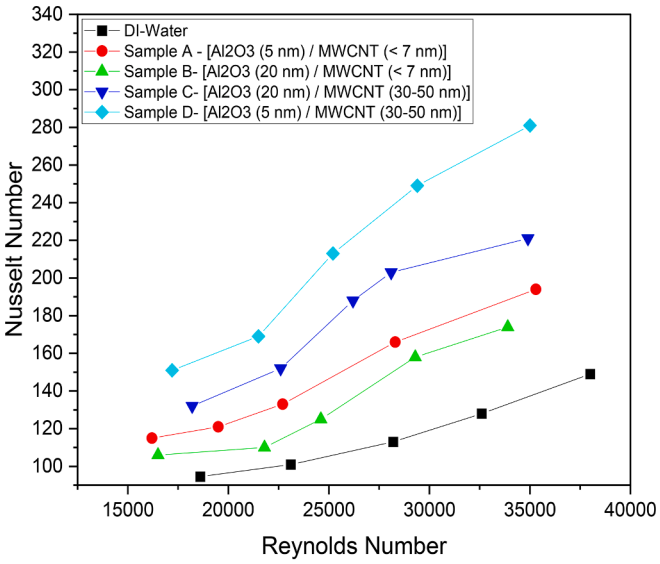


(a)

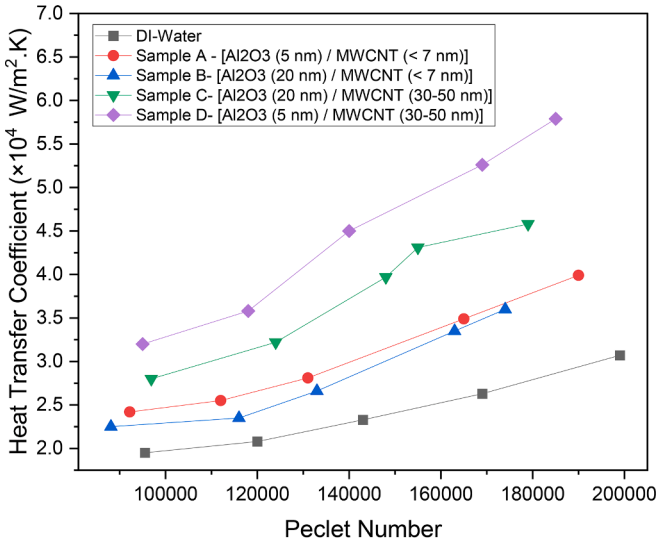


(b)

**Fig. 8.** Impact of Different Particle Size on Heat Transfer Performance for Continuous Jet cooling Condition.

motion. Hence, nanoparticles in Sample 'D' followed by 'C' had better convective heat transport mechanism compared to the other fluid because of their nanoparticle size. It is important to highlight the remarkable performance of all nanofluids in comparison to water across all flow rates under consideration.

### 3.3. *Continuous and pulsating jet cooling on the heat transfer*

Furthermore, a comparative analysis of the cooling performance of the respective fluids was conducted under continuous and pulsating jet impingement cooling conditions. The findings, illustrated in Fig. 9 **(a)-(e)**, elucidate a significant enhancement in heat transfer behavior with pulsating jet impingement as the flow Reynolds number rises. Nevertheless, a minor discrepancy arose in the case of sample 'D', where both jet cooling conditions exhibited a slight convergence in heat transfer behavior within the Reynolds number range of 24000 to 30000.

Among the pulsating jet cooling cases for samples A-D, it appears as though the influence of nanoparticle sizes was negligible at low flow

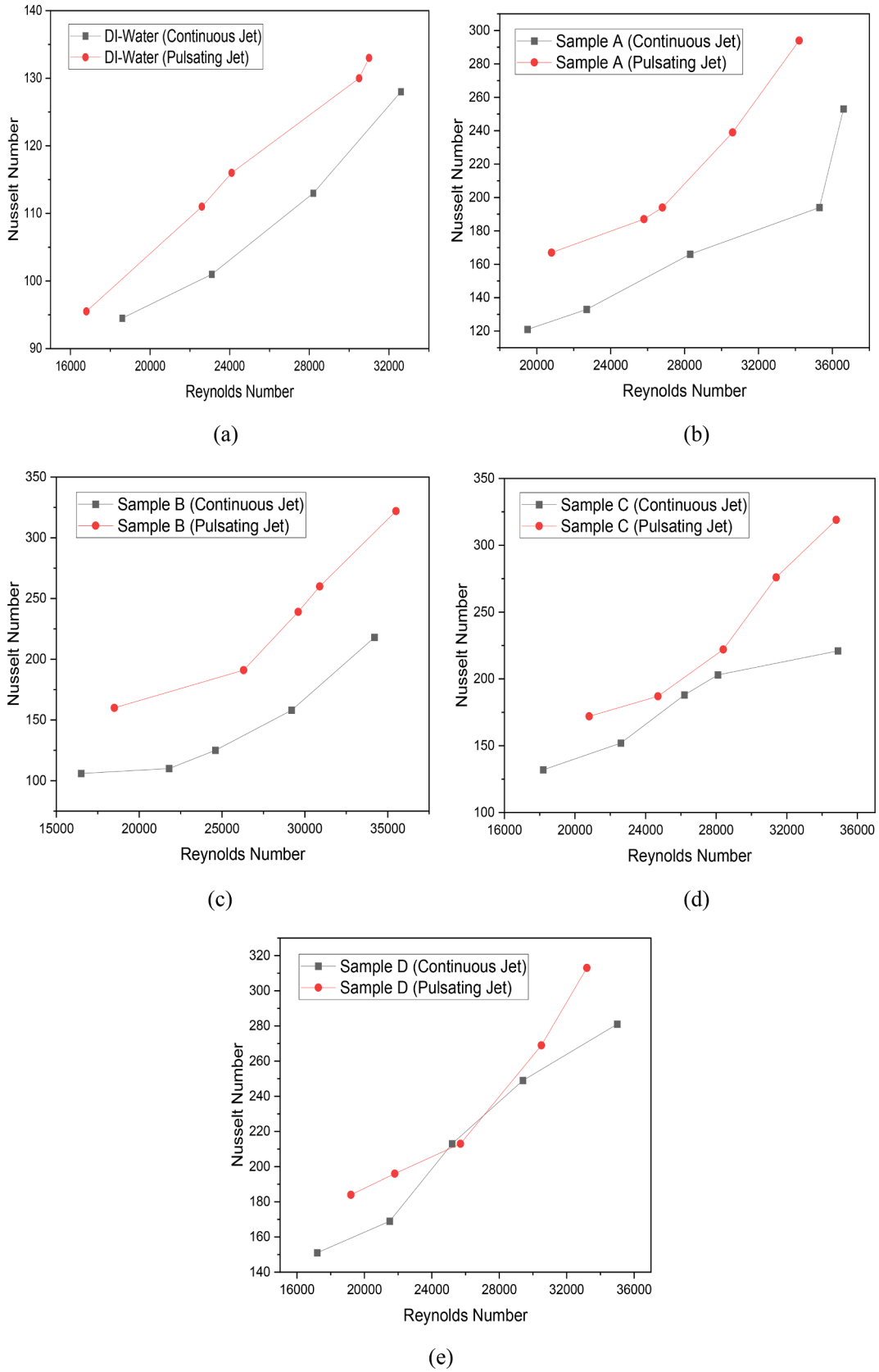


**Fig. 9.** Comparative heat transfer performance of the continuous and Pulsating Jet cooling.

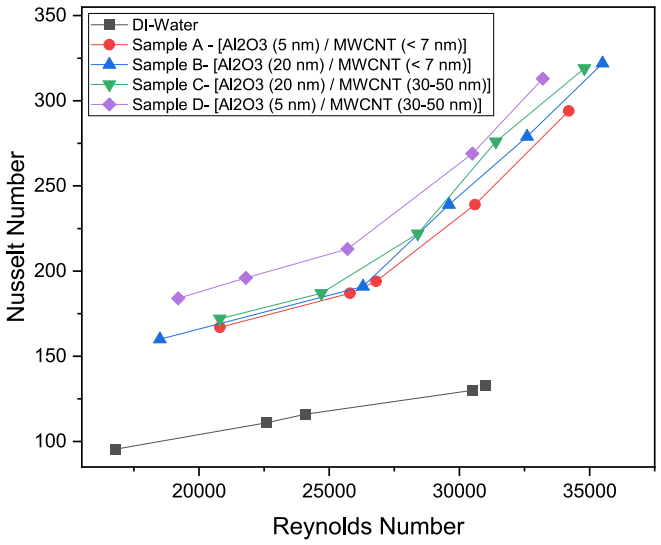


**Fig. 10.** Impact of Different Particle Size on Heat Transfer Performance for Pulsating Jet cooling Condition.

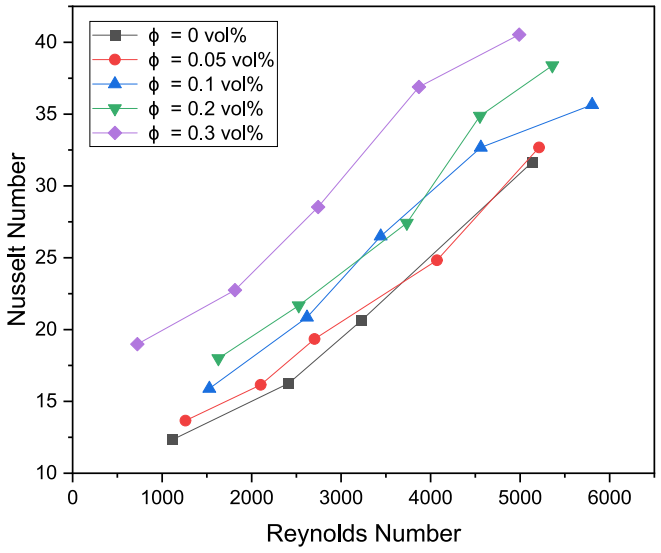


**Fig. 11.** Influence of Nanofluid concentration considering sample "D".

rates and slightly different at higher Reynolds numbers, except for sample D, which exhibits slight differences across varied flow rates. The findings, as depicted in Fig. 10, illustrate this observation. Altogether, it can be partially concluded that the effect of nanoparticle size is less significant for pulsating nanofluid jet impingement cooling conditions.

### 3.4. Nanofluid concentration influence on heat transfer

The investigation into the impact of nanofluid volume fraction, which denotes the concentration of nanoparticles within the base fluid, was conducted meticulously, with a specific focus on sample 'D', recognized as the most efficient nanofluid among the samples featuring diverse nanoparticle combinations. This comprehensive analysis presented in Fig. 11 spanned a Reynolds number range from 500 to 6000. By closely examining the thermal performance of different concentrations of nanofluid sample 'D', a profound understanding emerged regarding the pivotal role of nanofluid concentration as a significant influencing parameter. This scrutiny revealed that variations in nanofluid concentration wielded substantial influence over the overall thermal performance, emphasizing the critical role played by concentration levels in shaping the heat transfer characteristics of nanofluid systems. However, it is noteworthy that certain nanofluid volume fractions exhibited nearly similar heat transfer performances, rendering the influence of nanoparticle concentration somewhat unpredictable.

### 3.5. Development of Mathematical Corelation equation

According to Awe et al. [30], Machine Learning algorithms have been employed to generate correlations capable of predicting or forecasting the future occurrence of the factors under study. In heat transfer studies, they analyze complex datasets to identify key factors influencing performance. Their application enables optimization of system parameters and fosters innovative thermal management solutions.

We extended the analysis by using linear regression to investigate the relationship between key fluid parameters: Reynolds number (Re) and nanofluid volume fraction (ϕ), and heat transfer performance (Nusselt number). This analysis specifically focused on a continuous jet cooling scenario with a dimensionless nozzle-to-target gap (H/D) of 4. Through this analysis, we organized the data and applied a linear regression model to establish a line of best fit using Python Jupyter notebook. By doing so, we obtained coefficients that quantify the magnitude of influence exerted by each variable on the Nusselt number (Nu). The resulting model equation is presented as **Equation (13)**, encapsulates these relationships, and provides valuable insights into the dynamics of heat transfer in our experimental setup.

$$Nu = 0.0051.Re + 34.886.\phi + 4.128 \quad (13)$$

Moreover, the assessment of the model's predictive capabilities was conducted using evaluation metrics, namely the Mean Squared Error (MSE) and R-squared ($R^2$), employing the same Python code. The MSE of 1.345 indicates minimal deviation between actual Nusselt number and the predicted Nusselt number values, signifying the accuracy of the model predictions. Furthermore, an $R^2$ score of 0.985 suggests that approximately 98.5 % of the variance in Nusselt number (Nu) can be elucidated by the linear relationship with Reynold number (Re) and nanofluid volume fraction (ϕ). This robust model's performance underscores the influential role of Reynolds number and nanofluid volume fraction in modulating convective heat transfer rates, highlighting their significance in nanofluid heat transfer applications. The visualization depicted in Fig. 12, showcasing the close alignment between actual and predicted Nu values, reaffirms the reliability of the model and its potential to enhance our comprehension of heat transfer phenomena in nanofluid systems.

### 3.6. Variables Feature-Importance with Machine learning classifiers

As nanofluid jet impingement cooling becomes increasingly employed in thermal engineering applications due to its enhanced heat transfer properties, understanding the interplay between key variables; nanofluid particle-size combination (NF), pulsating jet impingement (P), nanofluid concentration (ϕ) and Reynolds number (Re), becomes paramount.

In this section we aimed to evaluate the predictive efficacy of machine learning classifiers in identifying the variables that most significantly influence thermal performance, specifically focusing on the Nusselt number (Nu), within the context of nanofluid jet impingement cooling. Through a comprehensive analysis, the study evaluates machine learning classifiers such as Support Vector Machines (SVM), Random Forest, Gradient Boosting, and Logistic Regression, shedding light on their effectiveness in delineating binary classifications of Nu based on predetermined thresholds.

Considering the accuracy plot presented in Fig. 13, logistic regression, followed by the SVMs had the least accuracy for classifying the variables influencing the thermal performance. However, the robust performance exhibited by Random Forest and Gradient Boosting

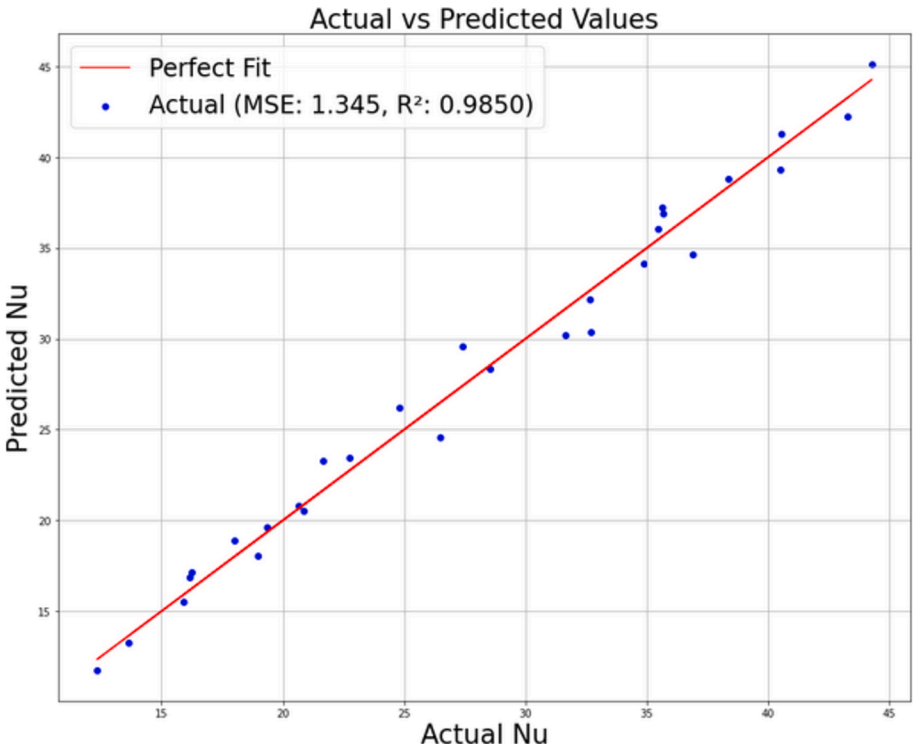


**Fig. 12.** Comparison of Experimental Nu and Model Predicted Nu.

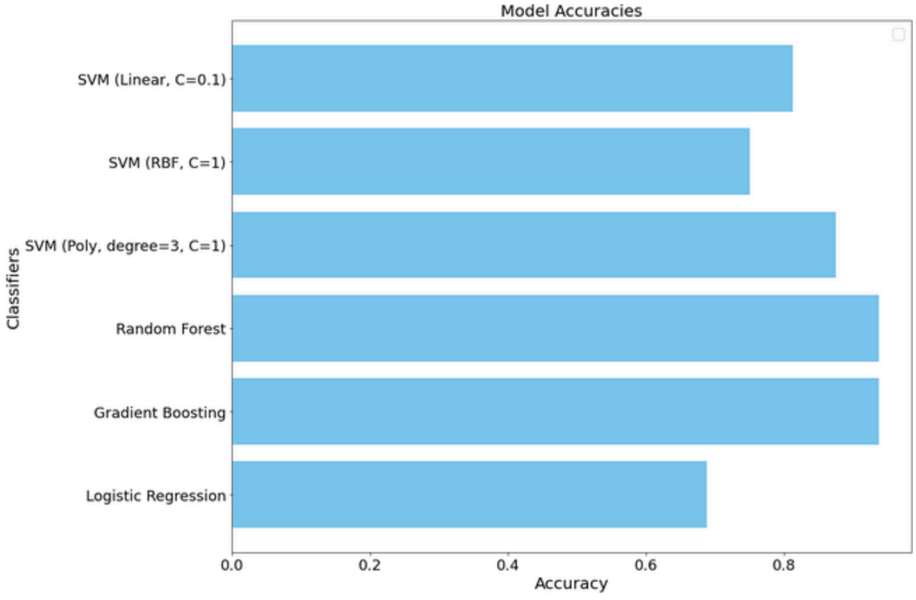


**Fig. 13.** Accuracy Plot for the Different Classifiers.

**Table 3**
Machine Learning Algorithm Precision Chart.

| Model | RMSE | MAE | R2 |
|---|---|---|---|
| SVM (Linear) | 38.823995 | 27.000023 | 0.835341 |
| SVM (RBF) | 83.721651 | 71.442123 | 0.234297 |
| SVM (Poly, degree = 3) | 48.946444 | 41.666988 | 0.738286 |
| Random Forest | 17.632549 | 12.60744 | 0.966036 |
| Gradient Boosting | 11.347081 | 8.146334 | 0.985935 |
| Logistic Regression | 28.508697 | 22.72381 | 0.911215 |

classifiers make them fit for predicting the variable feature importance for this study as their accuracy is almost unity (1).

The remarkable accuracy and minimal error margins in Nusselt number prediction is further presented in Table 3. This results also highlights that logistic regression, followed by the SVMs had the least $R^2$ values and the highest root mean square error (RMSE) and mean absolute error (MAE); implying that these classifiers would least predict the parameter influencing the thermal performance. Meanwhile, the least RMSE and MAE, and the highest $R^2$ values corresponds to Random Forest and Gradient Boosting classifiers. Hence, they would have the best proficiency in capturing intricate data patterns in this study, thus

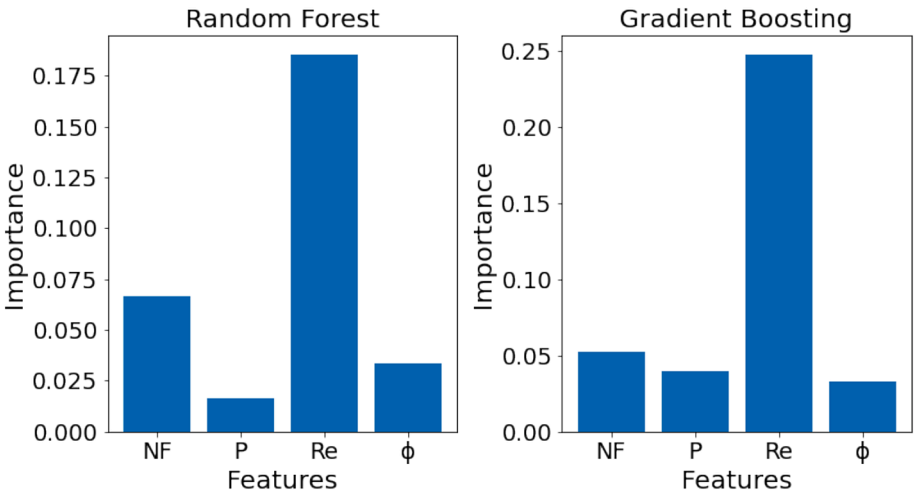


**Fig. 14.** Feature Importance Plot for the Best Classifiers.

offering promising avenues for precise thermal performance feature importance estimations.

Furthermore, using the best identified classifiers (Random Forest and Gradient Boosting) we delve into the nuanced hierarchy of variable influence. The result reveals that flow Reynolds number is the most dominant factor influencing the Nusselt number variations as seen in Fig. 14. Subsequently, nanofluid particle-size combination (NF) emerges as a significant contributor, elucidating its role in modulating heat transfer characteristics. Interestingly, pulsating jet impingement (P) and nanofluid volume fraction (ϕ) exhibits lesser and almost equal overall impact, as demonstrated comparably from their importance for both Random Forest and Gradient Boosting classifier, underscoring their relevance in certain predictive contexts.

## 4. Conclusion

In conclusion, this study comprehensively investigated the impact of nanoparticle size and pulsating jet cooling on heat transfer performance in hybrid nanofluids, specifically focusing on a simulated heat sink aligned to a PV cell's back plate. Key findings from our research include:

i. The thermal performance of the jet impingement cooling system (Nusselt number) was proportional to the flow Reynolds number, nanofluid volume fraction, nanoparticle-size combination and pulsation of the jet.
ii. The nanofluid sample D {$Al_2O_3$ (5 nm) and MWCNT (30–50 nm)} demonstrated superior heat transfer performance, indicating its potential as the most effective nanofluid among the samples.
iii. Nanoparticle size, nanofluid concentration, and pulsating jet cooling were identified as significant factors influencing heat transfer efficiency.
iv. The highest heat transfer enhancement was observed at the maximum volume fraction ($\phi = 0.3$ vol%) for the $Al_2O_3$-MWCNT/water hybrid nanofluid (Sample D) under pulsating jet cooling conditions.
v. Reynolds number emerged as the most prominent variables influencing the Nusselt number, followed by the nanofluid particle-size combination from the machine learning classifications.
vi. The Pulsating jet and the nanofluid volume fraction had approximately the same influence on the thermal performance as predicted from the machine learning classifications.
vii. The Random Forest and Gradient Boosting classifiers exhibited robust performance in predicting Nusselt numbers, offering promising avenues for precise heat transfer coefficient estimations.

These findings highlight the importance of nanoparticle characteristics and cooling methodology in optimizing heat dissipation, with implications for sustainable energy innovation and engineering solutions. Further research could delve into additional variable to refine optimization strategies and broaden the applicability of magnetic pulsating jet impingement cooling in various thermal management applications.

## Declaration of competing interest

The authors declare that they have no known competing financial interests or personal relationships that could have appeared to influence the work reported in this paper.

## Acknowledgement

This research was conducted at the Nanofluid laboratory of the University of Pretoria. The technical support of the Mr. Chris Govender and Mr. Donald Keetse is highly appreciated. Data analysis and machine learning was carried out in conjunction with LISA 2020 Global Network, USA.

## Data availability

Data will be made available on request.

## References

[1] M.A. Green, Third generation photovoltaics: solar cells for 2020 and beyond, Phys. E Low-Dimensional Syst. Nanostructures 14 (1–2) (2002) 65–70, https://doi.org/10.1016/S1386-9477(02)00361-2.
[2] Y. Xie, et al., Exergy performance assessment of a novel air-cooled photovoltaic thermal collector with a double serpentine runner, Appl. Therm. Eng. 236 (2024) 121330, https://doi.org/10.1016/J.APPLTHERMALENG.2023.121330.
[3] A. Aydın, İ. Kayri, H. Aydin, Electrical and thermal performance enhancement of a photovoltaic thermal hybrid system with a novel inner plate-finned collective cooling with different nanofluids, Int. J. Green Energy (2024), https://doi.org/10.1080/15435075.2023.2201345.
[4] A. Torbatinezhad, M. Rahimi, A.A. Ranjbar, M. Gorzin, Performance evaluation of PV cells in HCPV/T system by a jet impingement/mini-channel cooling scheme, Int. J. Heat Mass Transf. 178 (2021) 121610, https://doi.org/10.1016/J.IJHEATMASSTRANSFER.2021.121610.
[5] G. Huang, J. Xu, C.N. Markides, High-efficiency bio-inspired hybrid multi-generation photovoltaic leaf, Nat. Commun. 14 (1) (2023) 1–10, https://doi.org/10.1038/s41467-023-38984-7.

[6] E.O. Atofarati, M. Sharifpur, J.P. Meyer, Pulsating nanofluid-jet impingement cooling and its hydrodynamic effects on heat transfer, Int. J. Therm. Sci. 198 (2024) 108874, https://doi.org/10.1016/J.IJTHERMALSCI.2023.108874.
[7] U. Akdag, S. Akcay, N. Un, M. Danismaz, Experimental investigation of the heat transfer characteristics of a synthetic annular jet impingement on a flat surface, Exp. Heat Transf. (2024), https://doi.org/10.1080/08916152.2024.2356165.
[8] U. Akdag, M.A. Komur, S. Akcay, Prediction of heat transfer on a flat plate subjected to a transversely pulsating jet using artificial neural networks, Appl. Therm. Eng. 100 (2016) 412–420, https://doi.org/10.1016/J.APPLTHERMALENG.2016.01.147.
[9] H.M. Hofmann, D.L. Movileanu, M. Kind, H. Martin, Influence of a pulsation on heat transfer and flow structure in submerged impinging jets, Int. J. Heat Mass Transf. 50 (17–18) (2007) 3638–3648, https://doi.org/10.1016/J.IJHEATMASSTRANSFER.2007.02.001.
[10] H. Yadav, A. Agrawal, A. Srivastava, Mixing and entrainment characteristics of a pulse jet, Int. J. Heat Fluid Flow 61 (Oct. 2016) 749–761, https://doi.org/10.1016/J.IJHEATFLUIDFLOW.2016.08.006.
[11] H. Yadav, A. Agrawal, Effect of pulsation on the near flow field of a submerged water jet, Sadhana - Acad. Proc. Eng. Sci. 43 (3) (2018) 1–8, https://doi.org/10.1007/S12046-018-0814-1/FIGURES/3.
[12] H. Yadav, A. Agrawal, Effect of vortical structures on velocity and turbulent fields in the near region of an impinging turbulent jet, Phys. Fluids. 30 (3) (2018), https://doi.org/10.1063/1.5001161/105822.
[13] E. O. Atofarati, S. Mohsen, and J. P. Meyer, 2024 "Parametric influences on nanofluid-jet cooling heat transfer," in *Nanofluids: Preparation, Applications and Simulation Methods*, vol. 1, Elsevier, pp. 351–398.
[14] M. Javidan, A.J. Moghadam, Effective cooling of a photovoltaic module using jet-impingement array and nanofluid coolant, Int. Commun. Heat Mass Transf. 137 (2022) 106310, https://doi.org/10.1016/J.ICHEATMASSTRANSFER.2022.106310.
[15] H.A. Hasan, K. Sopian, A.H. Jaaz, A.N. Al-Shamani, Experimental investigation of jet array nanofluids impingement in photovoltaic/thermal collector, Sol. Energy 144 (2017) 321–334, https://doi.org/10.1016/J.SOLENER.2017.01.036.
[16] S. Bin Suja, M.R. Islam, Z.U. Ahmed, Swirling jet impingements for thermal management of high concentrator solar cells using nanofluids, Int. J. Thermofluids. 19 (2023) 100387, https://doi.org/10.1016/J.IJFT.2023.100387.
[17] F. Selimefendigil, H.F. Öztop, Pulsating nanofluids jet impingement cooling of a heated horizontal surface, Int. J. Heat Mass Transf. 69 (2014) 54–65, https://doi.org/10.1016/J.IJHEATMASSTRANSFER.2013.10.010.
[18] P. Li, D. Guo, R. Liu, Mechanism analysis of heat transfer and flow structure of periodic pulsating nanofluids slot-jet impingement with different waveforms, Appl. Therm. Eng. 152 (2019) 937–945, https://doi.org/10.1016/J.APPLTHERMALENG.2019.01.086.
[19] S. Maatoug, et al., Pulsating multiple nano-jet impingement cooling system design by using different nanofluids for photovoltaic (PV) thermal management, Case Stud. Therm. Eng. 41 (2023), https://doi.org/10.1016/J.CSITE.2022.102650.
[20] E.O. Atofarati, M. Sharifpur, J. Meyer, Hydrodynamic effects of hybrid nanofluid jet on the heat transfer augmentation, Case Stud. Therm. Eng. 51 (2023) 103536, https://doi.org/10.1016/J.CSITE.2023.103536.
[21] N. Wilken, M. Sharifpur, E.O. Atofarati, J.P. Meyer, Experimental study on transient and steady-state impinging jet cooling condition with TiO2-Water nanofluids, Case Stud. Therm. Eng. 57 (May 2024) 104301, https://doi.org/10.1016/J.CSITE.2024.104301.
[22] J.V. Sengers, J.T.R. Watson, Improved international formulations for the viscosity and thermal conductivity of water substance, J. Phys. Chem. Ref. Data 15 (4) (Oct. 1986) 1291–1314, https://doi.org/10.1063/1.555763.
[23] J. Çengel, A.G. Yunus, Afshin, Heat and mass transfer in SI Units: fundamentals and applications, 6th ed., MCGraw Hill, 2020.
[24] E.O. Atofarati, Investigation into heat transfer enhancement using AL2O3-MWCNT hybrid nanofluids in jet cooling, University of Pretoria, Hatfield, South Africa, 2024.
[25] R. Padiyaar, S. J. K. S, M. Mahdavi, M. Sharifpur, J.P. Meyer, Experimental and numerical investigation to evaluate the thermal performance of jet impingement surface cooling with MWCNT/Al2O3-deionized water hybrid nanofluid, Int. J. Therm. Sci. 184 (2023) 108010, https://doi.org/10.1016/J.IJTHERMALSCI.2022.108010.
[26] R.J. Moffat, Describing the uncertainties in experimental results, Exp. Therm. Fluid Sci. 1 (1) (1988) 3–17, https://doi.org/10.1016/0894-1777(88)90043-X.
[27] S.J. Kline, The purposes of uncertainty analysis, Trans. ASME 107 (1985) 154.
[28] O. Manca, D. Ricci, S. Nardini, G. Di Lorenzo, Thermal and fluid dynamic behaviors of confined laminar impinging slot jets with nanofluids, Int. Commun. Heat Mass Transf. 70 (2016) 15–26, https://doi.org/10.1016/j.icheatmasstransfer.2015.11.010.
[29] S. Abishek, R. Narayanaswamy, Low frequency pulsating jet impingement boiling and single phase heat transfer, Int. J. Heat Mass Transf. 159 (2020) 120052, https://doi.org/10.1016/J.IJHEATMASSTRANSFER.2020.120052.
[30] O.O. Awe, E.O. Atofarati, M.O. Adeyinka, A.P. Musa, E.O. Onasanya, Assessing the factors affecting building construction collapse casualty using machine learning techniques: a case of Lagos, Nigeria, Int. J. Constr. Manag. (2023), https://doi.org/10.1080/15623599.2023.2222966.